A statistically complete survey for arc-like features in images of distant rich clusters of galaxies

I. Smail,[1] R. S. Ellis,[1] M. J. Fitchett,[1] H. U. Nørgaard-Nielsen,[2] L. Hansen[3] and H. E. Jørgensen[3]

[1] *Department of Physics, University of Durham DH1 3LE*
[2] *Danish Space Research Institute, Lyngby, Copenhagen*
[3] *University Observatory, Østervolgåde, Copenhagen*

SUMMARY

Using data from an earlier search for supernovae in distant clusters, we have constructed a homogeneous set of V images for 19 rich clusters of mean redshift $\bar{z} = 0.32$. By considering the images above a fixed surface brightness limit, we have analysed the data for extended arc-like features which might arise from gravitational lensing of background sources. A list of 20 candidate arcs is presented. We examine the usefulness of such a catalogue for deriving the background source redshift distribution, $N(z)$. Whilst the number and shape distribution of arc candidates is consistent with the lensing hypothesis, cluster velocity dispersions of very high precision would be needed to provide useful constraints on the fraction of high-redshift galaxies to faint limits. We show how, in principle, a likelihood ratio test based on the radial distribution of arcs in a single well-studied cluster could determine whether a significant fraction of the faint galaxy population is at high redshift. This test also provides a means of determining accurate cluster velocity dispersions at any redshift.

1 INTRODUCTION

If the arc-like features seen in long-exposure images of moderate redshift clusters of galaxies (Fort *et al.* 1988; Tyson, Valdes & Wenk 1990) arise from gravitational lensing of background sources, their statistics might be used to constrain both the mass distribution in the lensing clusters (which is difficult to obtain by other methods) and the redshift distribution of the population of faint field galaxies unobtainable by conventional spectroscopy. The arc phenomenon is sufficiently new that it has been regarded largely as a demonstration of gravitational lensing, but our aim is to *use* arcs as a cosmological tool.

The arcs detected fall into two categories. First, there are *giant* arcs, e.g. those in Abell 370 (Soucail *et al.* 1988) and C12244 − 02 (Lynds & Petrosian 1989), which are sufficiently extended that they cannot easily be understood as normal galaxy images. Although the number of giant arcs is small, in those few cases where spectroscopy has been possible, the lensing hypothesis appears to be confirmed (see Fort 1990).

Secondly, there are the smaller features termed 'arclets'. Such arclets are often apparent only after the subtraction of deep frames taken in different passbands (Fort *et al.* 1988; Tyson *et al.* 1990), where their strikingly blue colours and orientation with respect to the cluster centre are taken to be further evidence of a lensing phenomenon. With one exception (the isolated arc A5 in Abell 370 − Soucail *et al.* 1990), spectroscopy is not yet available for the arclet population, so the lensing hypothesis, whilst plausible, is not strictly confirmed. For example, a significant fraction of arclets could be edge-on blue spirals at any redshift.

Grossman & Narayan (1988) and Nemiroff & Dekel (1989) demonstrated that for each giant arc there should be many arclets and that the *occurrence rate* for arcs of different sizes would test the lensing hypothesis further, and might add a new probe of the mass distribution in the cluster lenses and of the nature of the background source population. These articles explored the various probability distributions in some detail, but the absence of any well-defined observational sample precluded definitive conclusions.

Our aim in this paper is to examine such theoretical arguments in the context of a new sample of deep cluster images which has been systematically searched for arcs. The resulting catalogue of *candidate* arcs allows us to examine their potential for constraining the redshift distribution of faint field galaxies. We also compare this strategy of surveying a reasonably large number of clusters to moderate depths with the alternative approach where the surface density of background galaxies is raised to a statistically useful level in a

single cluster via much deeper integrations (*cf.* Tyson *et al.* 1990).

A plan of the paper follows. In Section 2 we describe a new observational database of distant clusters which has been constructed to maintain as uniform a detection limit for arcs and arclets as possible. Section 3 discusses the motivation for the statistical tests we have developed and demonstrates their application to our sample. The number of arcs found is consistent with the lensing hypothesis, but our cluster properties would need to be understood in much greater detail before strong constraints could be placed on the proportion of faint galaxies beyond the clusters. We develop a new technique which might resolve this problem but show that our current sample is too diverse for an effective application and briefly discuss how this could be applied to a more detailed analysis of one or more clusters. In Section 4 we consider the implications of this work and the prospective role which arcs may play in faint-object cosmology. We summarize our main conclusions in Section 5.

2 OBSERVATIONS

2.1 The Danish distant cluster sample

As part of the Danish distant supernova search (Hansen, Nørgaard-Nielsen & Jørgensen 1987; Couch *et al.* 1989), many *V* CCD frames of average exposure time ~ 1 hr were taken on the Danish 1.5-m telescope at La Silla, Chile for ~ 60 clusters with redshifts $0.2 < z < 0.5$ during the years 1987–89. Clusters were selected from the Abell catalogue (Abell 1958), its southern counterpart (Abell, Corwin & Olowin 1989) and the southern AAO distant cluser catalogue (Couch *et al.* 1990). The principal aim was to compare photometric observations of the clusters at different epochs in a search for faint supernovae (SNe). Since a Type Ia supernova could occur at any lunation, limiting magnitudes of $V \sim 24$ were essential for each exposure. Hansen *et al.* (1989) and Nørgaard-Nielsen *et al.* (1989) discuss the faint SNe discovered and the implications for cosmology and the SN rate. Over the many runs at La Silla, the observing conditions varied. In the SN search, new frames were compared with those whose seeing matched most closely the current conditions. Different transparencies and small seeing mismatches were then allowed for by rescaling and smoothing one image using fiducial stars as calibrators prior to eventual comparison.

As a trial application of the Danish frames for finding faint arcs, we registered and median filtered several frames of the cluster Abell 370 (Plates 1 and 2, Fig. 1), testing for the detection of the arclet A5 (Soucail *et al.* 1990). We found that, provided the frames were restricted to those with measured seeing ≤ 1.5 arcsec FWHM and that an effective total integration time of 4–5 hr on the Danish 1.5-m telescope was secured, the arclet could be readily detected as an extended object. From photometry in several clusters, we determined that a 4-hr *V* integration in typical conditions can reliably reach a limiting surface brightness of $\mu_V \sim 26.0$ mag arcsec^{-2}.

Our cluster sample for this study consists, therefore, of those in the SN programme for which the total *V* integration time with seeing ≤ 1.5 arcsec is ≥ 4 hr. The 19 clusters that fall into this category are listed with their redshifts in Table 1.
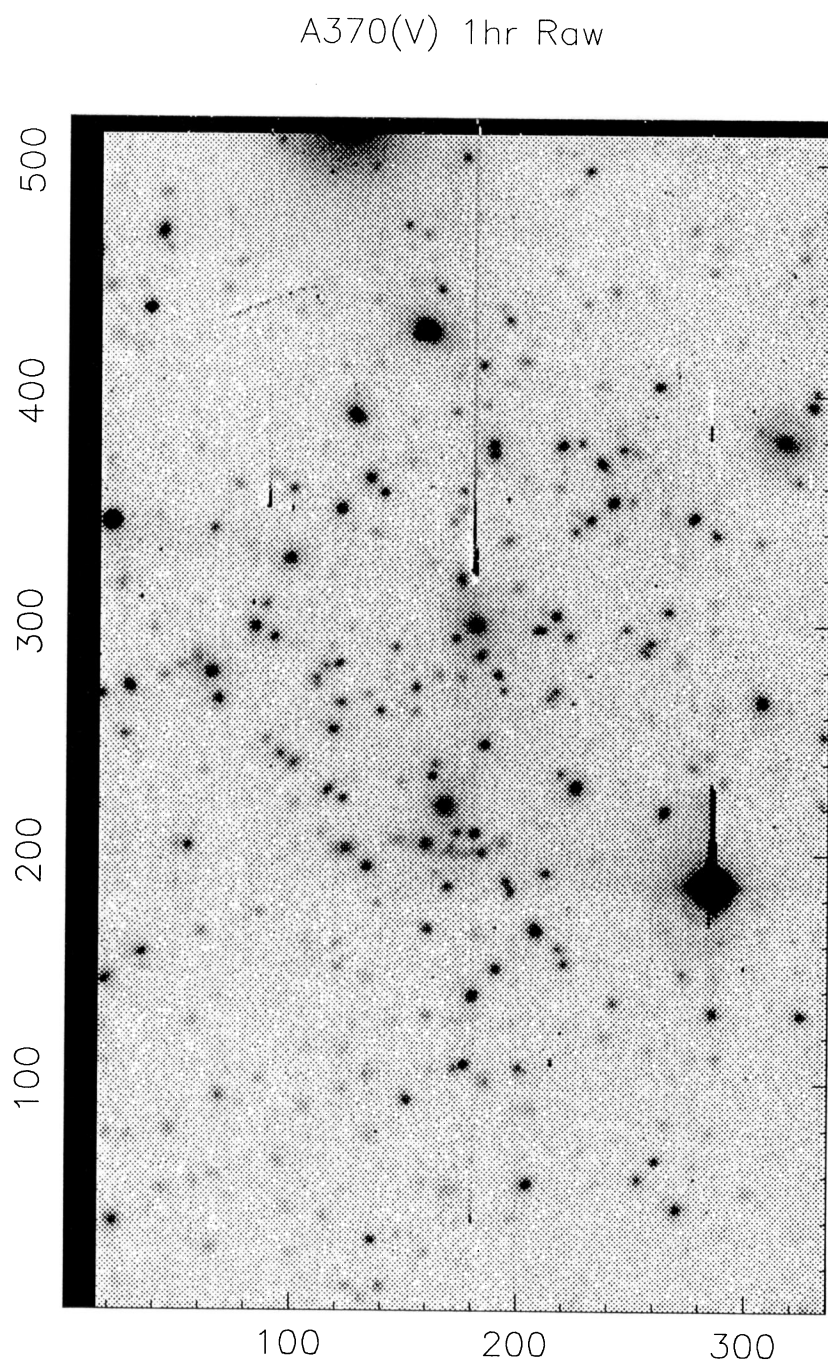

A370(V) 5HR MEDIAN
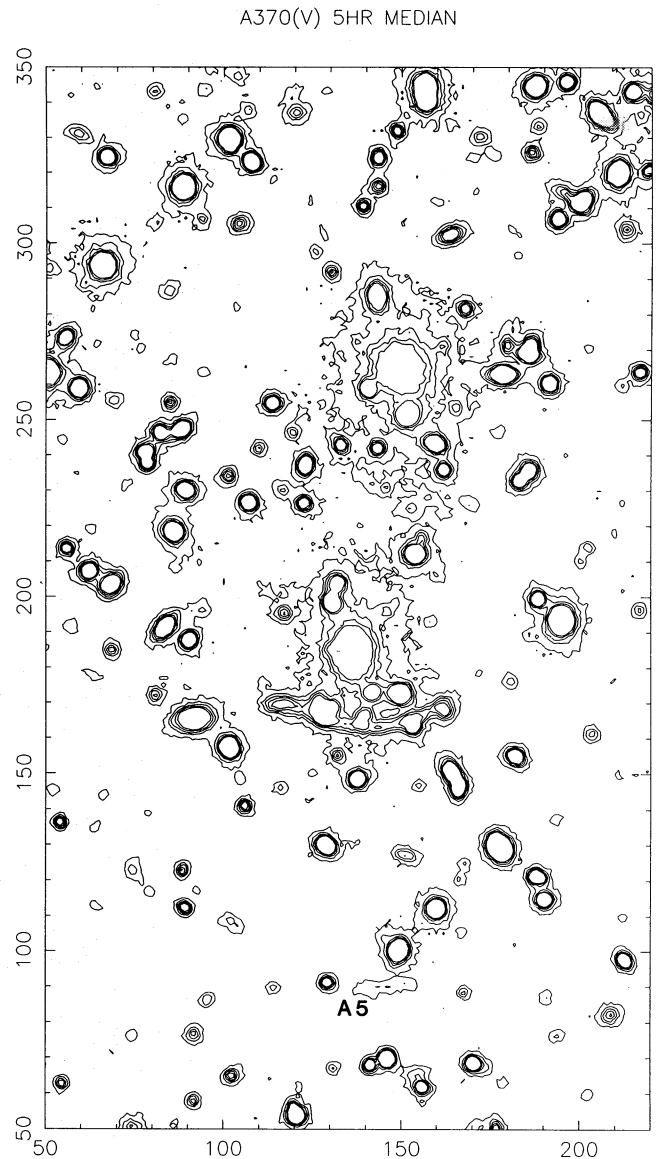
Figure 1. Contour map of Plate 2, showing a lowest isophote of $\mu_V = 26.0$ mag arcsec^{-2} and the arclet A5. The scale is in pixels, with 1 pixel = 0.47 arcsec.

Table 1. Danish cluster catalogue.

| Cluster	RA (1950)	Dec (1950)	Redshift	Exposure (hrs)
AC118	00 11 48	-30 42 00	0.31	8
Abell 222	01 35 04	-13 14 48	0.21	6
Abell 370	02 37 20	-01 47 51	0.37	8
J2175.23C	03 31 08	-39 16 49	0.43	8
J2183.27TL	03 45 37	-34 46 46	0.28	6
0346-45	03 46 49	-45 24 30	0.33	8
AC122	04 00 54	-27 20 49	0.21	8
J2001.21C	05 12 14	-48 21 54	0.42	8
J2090.7CL	10 02 12	-07 06 12	0.38	5
J1834.2TC	10 42 14	00 14 12	0.38	6
1141-28	11 41 40	-28 18 24	0.54	5
J1836.23T	13 40 35	00 13 20	0.42	5
J1836.14RC	13 41 11	-00 15 46	0.28	5
Abell 1942	14 35 55	03 52 24	0.22	6
AC106	20 06 00	-53 18 50	0.24	5
AC103	20 52 45	-64 51 22	0.31	5
Abell 2397	21 53 37	01 08 32	0.24	7
AC113	22 50 43	-33 59 27	0.22	6
AC114	22 56 00	-35 04 44	0.31	6

A370(V) 1hr Raw

Plate 1. Plates 1 and 2 show examples of the co-addition of Danish CCD frames taken at different epochs. Single 1-hr exposure.
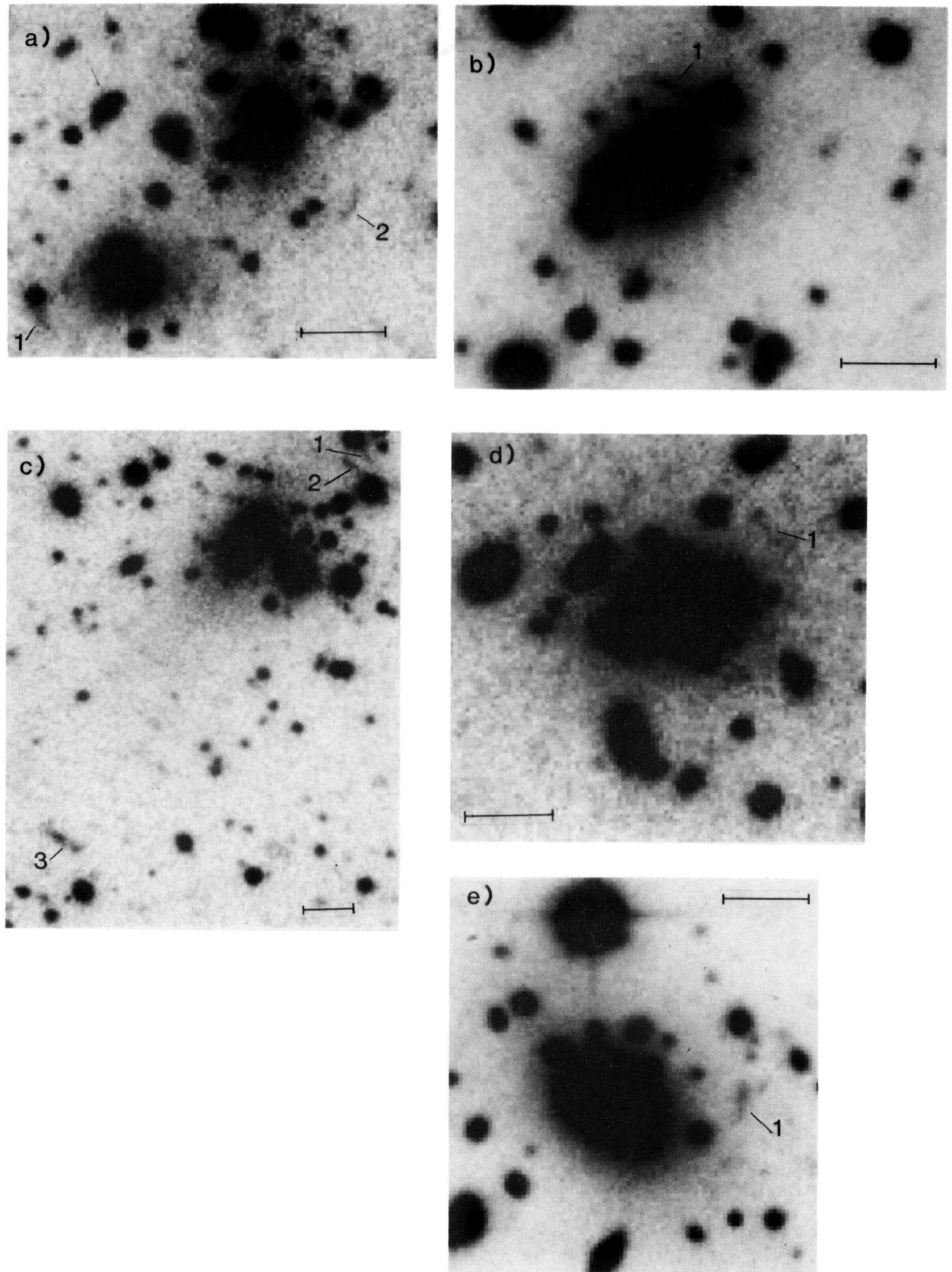
A370(V) 5hr Median
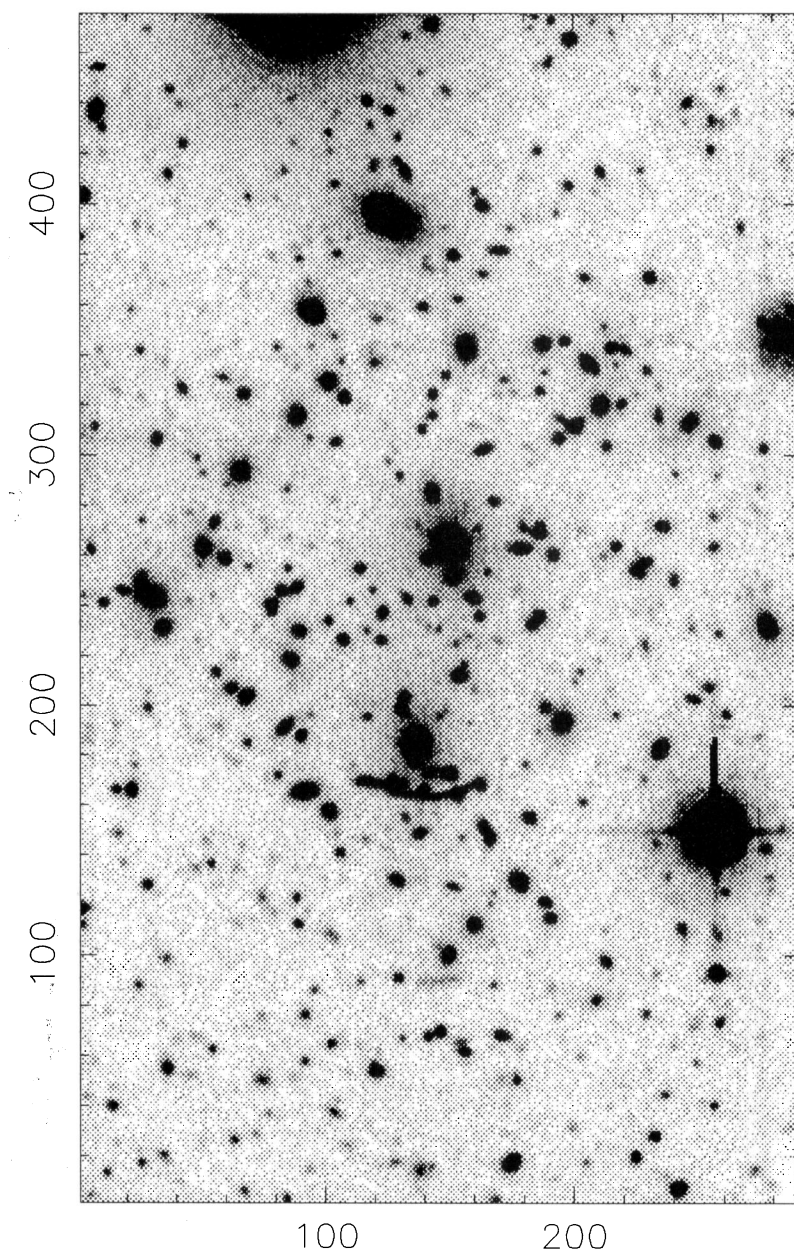
Plate 2. See caption to Plate 1 above. 5 × 1-hr exposures median filtered.

Plate 3. Examples of candidate arcs in five clusters processed according to the precepts of Section 2: (a) AC 118, (b) Abell 1942, (c) AC 114, (d) Abell 222 and (e) Abell 2397. The arc IDs corespond to those given in Table 2. North is up and east is left. The scale bars represent 10 arcsec.

The typical richness of a cluster entering this subset of the supernova search cluster sample can be calculated approximately from the source material for the clusters. The four Abell clusters are all distance 6, richness class 1 clusters, comparable to or exceeding Coma in richness. However, none has a reliable velocity dispersion or X-ray luminosity. Velocity dispersions are available for three of the six southern Abell *et al.* clusters from the extensive fibre spectroscopy of Couch & Sharples (1988). For these the mean line-of-sight dispersion in the rest frame is $\sigma_0 = 1483 \pm 566$ km s^{-1}, slightly in excess of that for Coma. The richnesses of the seven AAO clusters (J sequence numbers) can be estimated from their optical contrast against the background at their known redshift (*cf.* Couch *et al.* 1990). Several of these are weaker than Coma, so the mean is reduced slightly. Overall, it seems reasonable at this stage to conclude that the sample is statistically equivalent to 19 clusters comparable to Coma ($\sigma_0 \approx 800$–1000 km s^{-1}) at a mean redshift of $\langle z \rangle = 0.32 \pm 0.09$.

2.2 Homogeneity of the CCD survey

The individual V frames were first registered by a generalized rotation using the fiducial positions of typically seven to 10 stars. The resampled images were scaled to the same total sky count, stacked and median filtered to produce a single deep image free from cosmic rays and defects. The frame centres do not align perfectly but the common field is at least $\sim 2 \times 3$ arcmin^2 in all clusters. The gain in depth by this co-addition is illustrated in Fig. 1 where both the final Abell 370 image and a single 1-hr integration are compared at the same 2σ threshold of the background sky. The arclet A5, labelled in the figure, clearly emerges.

Before describing how the co-added cluster frames are searched for arc-like features, we need to define a self-consistent limiting surface brightness value and discuss how this might vary from frame to frame. Since the smallest arc with an axial ratio of, say, $a/b \geq 2$ that we can hope to recognize in frames of 1.5-arcsec seeing will occupy ~ 10 arcsec^2, we choose to cut all combined frames at a threshold of 2σ of the sky brightness on these scales: this corresponds typically to 1 per cent of the background sky.

Although the clusters were always observed in dark time, the varying night sky brightness and difference in total exposure time from one cluster to another will ensure that such a limiting surface brightness cut varies from cluster to cluster. This cannot be eliminated entirely without accurate photometric zero points which are not available in every cluster. Nevertheless, we demonstrate that the variation in the limiting surface brightness is small enough for the catalogue to be useful for our purposes. Of course, by virtue of averaging at least four frames taken at different times for each cluster, the sky brightness will approach the overall average value at La Silla during 1987–89.

The mean exposure time of 6.4 hr has a 1σ scatter of ~ 20 per cent which, together with airmass differences on the meridian, imply a spread of less than 0.15 mag in the surface brightness that corresponds to a constant signal-to-noise ratio. The absolute value of the sky brightness can be checked for three clusters containing good V photometric zero points (A1942, A370 and AC118) and these confirm a mean sky value of $\mu_V = 21.0 \pm 0.3$ mag arcsec^{-2}. We take this

range as representative of the 15 other clusters observed during the same period. In summary, therefore, by cutting at 2σ of the median sky value across the co-added image, our survey should maintain a strict surface brightness limit of $\mu_V = 26.0 \pm 0.3$ mag arcsec^{-2}.

2.3 Identification of arc candidates

Both Grossman & Narayan (1988) and Nemiroff & Dekel (1989) showed in detail how lensing elongates an image by an amount that depends on the source and lens distances (z_s, z_{cl}), the lens mass (which can be represented by the line-of-sight velocity dispersion, σ_{cl}, in simple cases), and the true angular separation of the source and lens, θ_s. For an isothermal cluster, an intrinsically circular background source appears elongated such that the *minor* axis of the image equals the undistorted radius of the galaxy, and the *major* axis is elongated along the normal to the line joining the source and lens centre. Two observational parameters are crucial to any statistical analysis: the axial ratio $A = a/b$ of the lensed image, and the angular distance, d_c, of the arc candidate from the cluster centre (which will usually be quoted in arcsec).

Each processed frame was cut at a threshold of 2σ above the sky level (as discussed in Section 2.2) and examined visually for objects with axial ratios $A \geq 2$. This was deemed more appropriate than an automatic image analysis for several reasons. First, such algorithms are not suitable for the crowded fields and extensive envelopes near the cluster centres where arcs have often been found (e.g. Abell 963, Lavery & Henry 1988). Secondly, by examining the frames visually, the curvature of the arcs can also be assessed. Finally, in confusing situations the frames can be readily pushed to a lower threshold to clarify the reality or otherwise of defects or weak features.

The complete list of candidate arcs and their parameters is given in Table 2. In this list, the radius vector is calculated using the estimated optical centre of the cluster (in every case the brightest member), but it should be emphasized that this was done *after selection*. Since Abell 370 was included in the

Table 2. Arc catalogue ($A > 2$).

Cluster	Redshift	Arc ID	A	d_c^1 (arcsec)
AC118	0.31	AC118-1	2.9	13.7
AC118	0.31	AC118-2	3.6	21.4
AC118	0.31	AC118-3	2.5	10.9
A222	0.21	A222-1	4.7	12.2
A222	0.21	A222-2	2.6	14.1
A370	0.37	A370-1	12.3	26.3
A370	0.37	A370-2	4.0	63.7
J2183-27T	0.28	J2183-1	2.2	6.1
J2090-7CL	0.38	J2090-1	2.7	3.1
J2090-7CL	0.38	J2090-2	2.3	5.1
A1942	0.22	A1942-1	3.0	8.1
A1942	0.22	A1942-2	2.0	55.4
A1942	0.22	A1942-3	2.6	23.2
A2397	0.24	A2387-1	2.4	14.6
AC113	0.22	AC113-1	2.2	32.4
AC113	0.22	AC113-2	2.2	30.5
AC113	0.22	AC113-3	2.6	25.3
AC114	0.31	AC114-1	2.3	27.1
AC114	0.31	AC114-2	4.6	25.8
AC114	0.31	AC114-3	4.1	61.9

[1] Radius from cluster centre.

Danish SN search without any regard for its spectacular giant arc, we consider it appropriate to include this cluster in the sample.

Plate 3 shows the *V* images for those five clusters which, besides A370, contain the arc candidates with the largest distortions ($A \geq 3.5$). Whilst the majority of the candidates are, in fact, approximately normal to the cluster radius vector, it is clear that some are not. These could be spurious detections, or cases where the symmetry of the cluster potential is far from circular or elliptical.

To test the reliability of the candidate list, we would like to examine images in other passbands. Although *B* and *R* images were occasionally taken for the SN search, they are few in number and consequently their mean depth cannot match that of the prime *V*-band material. Further studies of these arcs are in progress, at optical and infrared wavelengths. For example the arc in A1942 has been detected in *K* (Aragón-Salamanca *et al.*, in preparation). The expected contamination rate in our sample has been estimated by analysing the ellipticity distribution of 10^5 objects in a 1 square degree randomly chosen field. The field used is an AAT prime focus b_J plate scanned by the COSMOS machine to a limiting magnitude of $b_J \sim 24.5$. The surface density of objects complying with our distortion and size criteria for the arcs is such that we would expect to find one edge-on interloper in every 200 clusters for this limiting surface brightness. Extrapolation using Tyson's (1988) number counts to our surface brightness limit of $\mu_V = 26$ mag arcsec^{-2} would give one interloper in every 40 clusters, i.e. 2 per cent of those in Table 2. Further evidence for the lack of contamination is given by the fact that, even though we have not emphasized the orientation of the arc candidates, the majority are tangentially aligned.

The only similar attempt to generate a statistically complete sample of arc candidates was that of Lynds & Petrosian (1989) who comment in their analysis of the Abell 370 and Cl2244 − 02 giant arcs that, during an examination of 58 clusters, they found only two examples of such giant arcs. Their 58 clusters covered a much wider range in redshift and they pointed out that both of these arcs occur in clusters with redshifts well above the median value for their sample ($\langle z \rangle = 0.23$). If their sample is restricted to the 27 clusters with $0.2 < z < 0.4$, the rate for the giant arcs would be such that one is seen in ≈ 8 per cent of the Abell clusters. This is somewhat higher than our rate for the largest arcs (which already depends heavily on the presence of Abell 370 justified above) but is probably within the statistical uncertainties. Since Lynds & Petrosian's images were taken in a variety of passbands with a much greater range of exposure times *depending on the cluster redshift*, our survey should be more homogeneous and more useful for the analysis below.

3 ANALYSIS

3.1 Motivation

A major hope with gravitational lensing is that the arc statistics will provide new constraints on the redshift distribution of background sources. In this section we develop techniques to address this question, using our new sample to demonstrate the sensitivity of various statistical probes to assumptions, e.g. about the lensing clusters themselves.

Recent work on the redshift distribution, $N(z)$, of faint galaxies has presented a dilemma. Multiple object spectroscopy on 4-m telescopes has generated redshift surveys of a few hundred galaxies to successively fainter limits of apparent magnitude. Broadhurst *et al.* (1988) used the AUTOFIB fibre optic system at the AAT to define $N(z)$ with 85 per cent completeness to a limit of $b_J = 21.5$, and Colless *et al.* (1990) used the LDSS multislit spectrograph with a similar completeness to $b_J = 22.5$. The resulting median redshift $\bar{z}$ hardly increases with apparent magnitude and implies that the bulk of the faint population to $b_J = 23$ lies below $z \sim 0.5$. Similar conclusions have been derived from surveys at Kitt Peak and CFHT (see Koo 1989; Cowie & Lilly 1990).

The discovery of a population of extremely blue *flat spectrum* sources emerging at $b_J = 23$ has led to speculation that this population, which rises to dominate the counts somewhat fainter, is significantly more distant (Cowie *et al.* 1989; Tyson 1988). Some support for this evidence is the preponderance at this stage of arcs with blue colours and Tyson *et al.*'s (1990) claim that only the blue population is distorted in deep cluster images. An upper redshift limit ($z \leq 3.0$) for this faint blue population has been provided by their detection in the ultraviolet (Guhathajurta, Tyson & Majewski 1990). However, if this hypothesis is correct, the onset of such a distant population must be very sudden in terms of apparent magnitude, since no high-redshift ($z > 1$) objects are currently seen in the spectroscopic surveys (Ellis 1990).

3.2 Approximating the selection function

Whereas galaxies are selected by apparent magnitude in the number counts and spectroscopic studies, the candidate arcs in Table 2 are found by virtue of their *surface brightness*, which is conserved in the lensing process. For the magnitude-limited samples, a *selection function* $\phi(z)$ is usually modelled on the basis of the present-day luminosity function of galaxies (Efstathiou *et al.* 1988) and certain assumptions about the effects of redshift and evolution. In this way the form of $N(z)$ can be estimated for any magnitude-limited sample, including one slightly fainter than the current limit of the redshift surveys.

Although it is possible, in principle, to calculate the selection function for a sample limited by surface brightness, this would demand more information on the present-day properties of galaxies than is currently available. For example, in addition to knowledge of the distribution of integrated luminosities of galaxies per unit volume, a good understanding would be required of the distribution of surface brightness profiles (their central values and forms) for which there remains considerable controversy because of observational selection effects (Phillipps, Disney & Davies 1990). Any predicted $N(z)$ for a sample, for example, limited at $\mu_V = 26.0$ mag arcsec^{-2}, would be based on highly uncertain initial assumptions.

Rather than introduce uncertain models, we adopt a much simpler approach. At the most basic level, the arc statistics are required to test whether the majority of faint blue objects are behind or in front of the clusters; the precise form of $N(z)$ is not required. As far as the limiting observational parameters are concerned, we can also estimate statistically that, if the magnification is a/b, a sample limited at $\mu_V = 26.0$ mag arcsec^{-2} in 1.5-arcsec seeing approximates an apparent-

magnitude-limited sample with $V \leq 26 - 2.5 \log(1.5a/b)$. For $a/b = 2$, our minimum criterion, this becomes $V \leq 25$.

At this limit, Tyson's (1988) b_J and R counts imply a surface density of 13.6 objects arcmin^{-2} of which 35 per cent have colours in the *flat-spectrum* category $b_J - I \leq 1.0$ as defined by Cowie & Lilly (1990). To examine whether arcs can place useful constraints on the likely redshift distribution of various subsets of the faint galaxy population we first propose the following two illustrative (and extreme) hypotheses.

(i) H_0: the flat-spectrum galaxies broadly share the same $N(z)$ as the non-evolving distribution, as suggested by Broadhurst *et al.* (1989) and Colless *et al.* (1990). Roughly speaking this would imply $\langle z \rangle \sim 0.55$ and the bulk of the population having $z < 1$.

(ii) H_1: the flat-spectrum galaxies all lie between $z = 1$ and 4 as suggested originally by Cowie *et al.* (1989). We will explore various distributions that place these galaxies within these redshift limits.

We parametrize the fraction of flat-spectrum objects to $V = 25$ as f_b. Cowie *et al.* (1989) claim that, regardless of their redshift, the surface density of this fraction of blue sources implies that the bulk of the metals were formed in this population. The null hypothesis, H_0, implies that the population co-exists with the remainder and is temporary in nature (e.g. by virtue of short-term bursts of star formation); the overall $N(z)$ being the no-evolution prediction. The alternative hypothesis, H_1, amounts to the statement that the flat-spectrum component is a cosmologically important one, perhaps associated with galaxy or disc formation in the remote past. In this case the fraction $(1 - f_b)$ without flat-spectrum colours is assumed to be a non-evolving population. Of course a host of intermediate possibilities exist. Our purpose here is to examine the sensitivity of various tests to these extreme hypotheses.

3.3 Lens models and robust arc parameters

The simplest cluster potential that might be considered is the singular isothermal sphere. Predictions for the effect of such a potential on the shapes of background galaxies have been made by Nemiroff & Dekel (1989). In this case the lensing geometry is straightforward – all light rays from the source are deflected through a constant angle α_0 at the cluster, where

$$\alpha_0 = 4\pi \left(\frac{\sigma_{cl}}{c}\right)^2 \sim 29 \left(\frac{\sigma_{cl}}{10^3 \text{ km s}^{-1}}\right)^2 \text{ arcsec.} \quad (1)$$

Every point on the source plane is moved an angular distance $\Delta = \alpha_0[1 - r(z_l)/r(z_s)]$ away from the cluster centre, where $r(z) = 2cH_0^{-1}(1 - 1/\sqrt{1 + z})$, assuming an $\Omega = 1$ universe with matter inside the beam to the cluster (see for example Turner, Ostriker & Gunn 1984). Intrinsically circular sources whose impact parameter lies close to the cluster centre will be distorted considerably, while sources with larger impact parameters will be distorted less. This simplified lensing geometry does not affect the width of the source. The singular isothermal sphere model is used in this paper to show the type of analysis that might be carried out. In Section 4 we will discuss its validity and other possible mass distributions.

This model gives the final shape of the image, A, and its distance from the cluster centre, d_c, as a function of the source redshift z_s, the lens redshift z_l, the source impact parameter, θ_S, and the cluster velocity dispersion, σ_{cl}. Given a set of clusters with known or assumed velocity dispersions and a hypothesized $N(z)$, this model predicts the observed number of arcs as a function of their distortion A, their distribution radially relative to the cluster centre or centres and their lengths (with some assumption on the intrinsic source size). Any of these quantities can be compared with the available data. The arc length distribution is probably not useful for comparing theory with observations since little is known about the intrinsic source size. The quantities A and d_c are, however, fairly easy to measure and not sensitive to such unknown quantities.

Calculation of the expected number of arcs is straightforward. Following Nemiroff & Dekel (1989), for a single cluster with a singular isothermal sphere mass distribution

$$N_{arc}(A > A_c) = \pi \alpha_0^2 (A_c - 1)^{-2} \Sigma_s J(\hat{N}, z_{cl}), \quad (2)$$

where

$$J(\tilde{N}, z_{cl}) = \int_{z_{cl}}^{\infty} \tilde{N}(z_s)[1 - r(z_{cl})/r(z_s)]^2 \, dz_s.$$

Here Σ_s is the surface density of objects down to the surface brightness limit of the sample and $\hat{N}(z_s)$ is the normalized redshift distribution of these sources [i.e. $\int \hat{N}(z_s) \, dz_s = 1$]. It is trivial to calculate from this formula the expected number of arcs for an ensemble of clusters, and for different hypothesized $\hat{N}(z_s)$. Notice that the integral is linear in $\hat{N}(z_s)$. Therefore a mixture of populations with a fraction f_b of
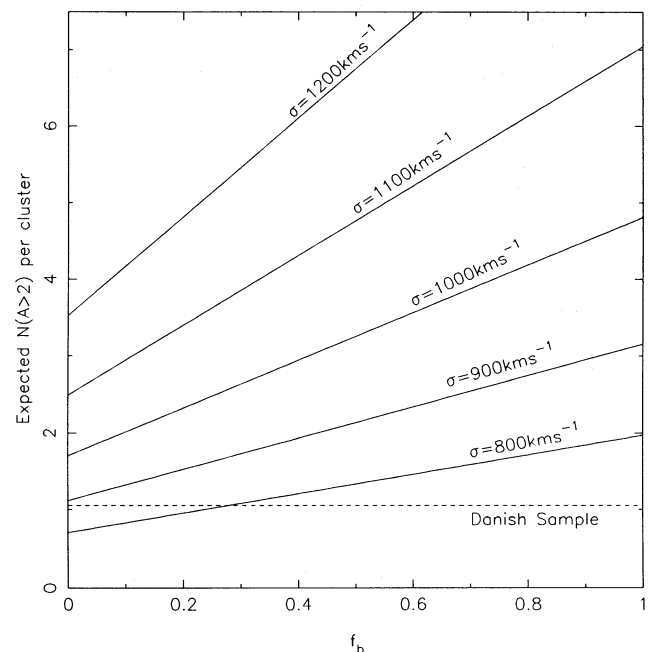
Figure 2. The predicted number of arcs with $A > 2$ as a function of the fraction of sources, f_b, placed at $z_b = 2$, plotted for various cluster velocity dispersions.
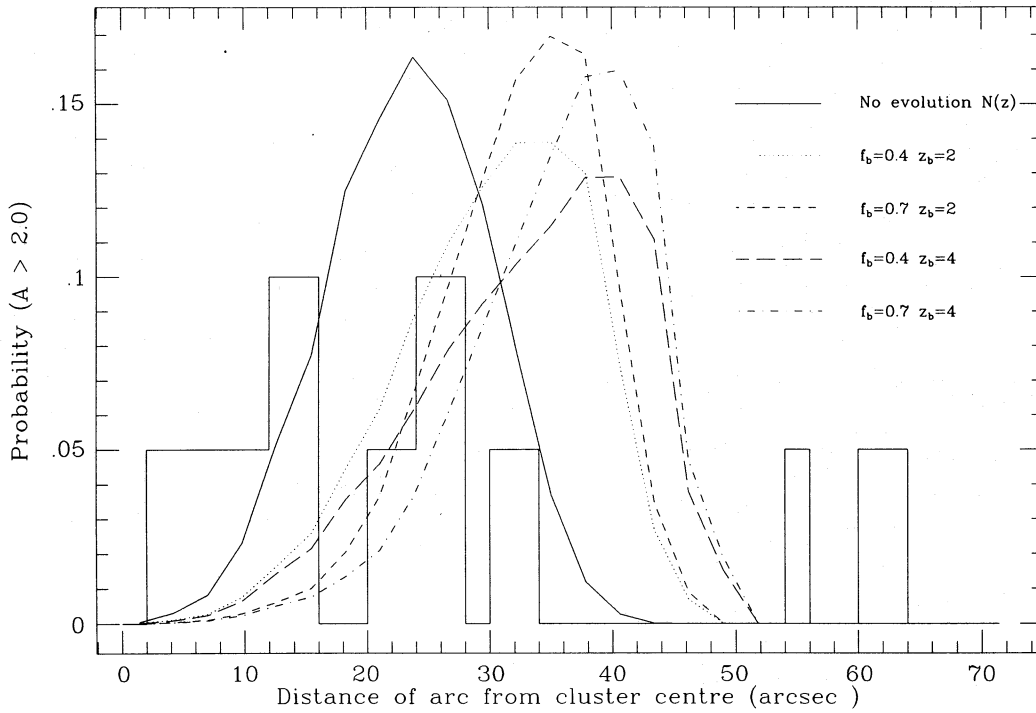
Figure 3. Predictions for the radial distribution of arcs with $A > 2$ for a cluster with velocity dispersion 1000 km s^{-1} and various hypothesized $N(z)$: the solid curve is for a no-evolution $N(z)$, while the other curves place various fractions, f_b, of the sources at various redshifts, z_b, and distribute the remainder according to the no-evolution prediction. The histogram of radial distances for the Danish data is also shown.

galaxies drawn from $\hat{N}_b(z_s)$ and the remaining $(1 - f_b)$ drawn from $\hat{N}(z_s)$ would give

$$N_{\mathrm{arc}}(A > A_c)$$
$$= \pi a_0^2 (A_c - 1)^{-2} \Sigma_s [(1 - f_b) J(\hat{N}, z_{\mathrm{cl}}) + f_b J(\hat{N}_b, z_{\mathrm{cl}})]. \qquad (3)$$

If σ_{cl} is known (say from X-ray data or a large sample of measured velocities in the cluster) and the cluster mass distribution is described by the singular isothermal sphere model then the number of arcs seen with distortions greater than some specified value could determine f_b.

Predicting the distribution of d_c is not quite so simple. The first step to note is that images of circular sources at z_s with distortions $A > A_c$ must lie in the annulus

$$d_c \in \{\Delta, \Delta[1 + (A_c - 1)^{-1}]\}.$$

Given that sources uniformly populate the region behind the cluster, one can then calculate the probability distribution for d_c within this annulus, and convolution of that with the source redshift distribution gives the final probability distribution of d_c for arcs with distortion $A > A_c$ as

$$\Phi(d_c) = \beta \int_{z_1(d_c)}^{z_2(d_c)} \frac{2\hat{N}(z_s)[d_c - \Delta(z_l, z_s, \sigma_{\mathrm{cl}})]}{\Delta(z_l, z_s, \sigma_{\mathrm{cl}})^2} \, dz_s \qquad (4)$$

where β is the normalizing constant and $z_1(d_c)$, $z_2(d_c)$ are respectively the solutions of the equations

$$d_c = [1 + (A_c - 1)^{-1}] \Delta(z_l, z_1, \sigma_{\mathrm{cl}})$$

and

$$d_c = \Delta(z_l, z_2, \sigma_{\mathrm{cl}}).$$

In this paper we have solved this integral by Monte Carlo simulation of the effect of our clusters on a background population.

3.4 Comparison of models with the Danish sample

There are two possible tests that can be carried out on the Danish arc sample. The simplest is to compare the number of arcs detected with $A > A_c$, $N_{\mathrm{arc}}(A > A_c)$, with that expected under the two hypotheses discussed above. The second is based on the distribution of the arc distances, $\Phi(d_c)$, from their cluster centres.

Suppose for example that one places a fraction f_b of galaxies at $z = 2$ with the remaining $(1 - f_b)$ distributed according to the standard no-evolution $N(z)$ predicted for a $V = 25$ mag limited sample. Using the formula from the previous section we have calculated the number of arcs with $A > 2$ expected for our ensemble of clusters, where each cluster has been assumed to have the same velocity dispersion. Adopting a source surface density of 13.6 arcmin^{-2} (Tyson 1988), the results for various σ_{cl} are shown in Fig. 2. The observed number of arcs, 20, is consistent with these predictions. Indeed one might be tempted to infer from this plot that a small fraction of high-redshift galaxies is preferred. However, these clusters are very unlikely to have equal velocity dispersions, and one can see from Fig. 2 that the relation between $N_{\mathrm{arc}}(A > A_c)$ and f_b depends strongly on the cluster velocity dispersion. The predicted number of arcs with $A > 2$ varies by a factor ~ 2 as f_b increases from 0 to 1, but $N_{\mathrm{arc}} \propto a_0^2 \propto \sigma_{\mathrm{cl}}^4$. Thus small errors ($\sim 20$ per cent) in the measurement of the cluster velocity dispersion can easily

mask the increased number of arcs expected due to the high-redshift population.

For the second test we again suppose that each cluster has the same (unknown) velocity dispersion and lies at the mean redshift of the sample, 0.32. The probability distribution of d_c for those arcs with $A > 2$ has then been calculated for a range of redshift distributions comprising the null distribution and four other distributions where a variable fraction f_b of the sources are placed at various fixed redshifts z_b. These probability distributions, $\Phi(d_c)$, are shown in Fig. 3 for a cluster velocity dispersion of $\sigma_{cl} = 1000$ km s^{-1}. On the same figure the Danish arc data probability distribution is shown. Clearly there is little agreement between any of these models and the data. Indeed there is no agreement for any velocity dispersion. The most likely cause of this discrepancy is the range of cluster velocity dispersions. The sample will be likely to contain clusters with high velocity dispersion, which give rise to large values of d_c, and with low velocity dispersion, which will not act as significant lenses at all. For this sample the distribution of d_c does not act to constrain the $N(z)$ of the faint sources. We note, however, that the *shape* of $\Phi(d_c)$ is different for each of these hypotheses and one might therefore, with a large sample of arcs in one cluster, be able to constrain $N(z)$ using the shape of this function. The larger the fraction of high-z objects, the more skew this function becomes.

There are other simple questions one can ask about this sample; for example, is the distribution of A consistent with that expected from lensing and are the number of arcs in each cluster consistent with the clusters having equal velocity dispersions? Independent of the cluster velocity dispersion we should find $N_{arc}(>A) \propto (A-1)^{-2}$, and the lack of dependence on σ_{cl} means that this should hold for the entire sample. A KS test on the observed distribution of A shows that the probability that it was drawn from the $N_{arc}(>A) \propto (A-1)^{-2}$ distribution is ~9 per cent. Whilst a low value, it remains consistent with the lensing hypothesis. Removal of the large arc in A370 has little effect on this probability.

On the second question, if all of the clusters did have the same velocity dispersion then the number of arcs seen in any cluster should have a Poisson distribution with a mean value of 20/19. The number of arcs in these clusters varies from 0 in several to maximally 8. A χ^2 test shows that this distribution is *not* consistent with the Poisson distribution at the < 1 per cent level. We have therefore effectively demonstrated why the above tests will not work on our sample in the absence of detailed knowledge about the clusters themselves.

One can show that, in order to obtain f_b to accuracy δf_b, the error on σ_{cl}, $\delta\sigma_{cl}$ must satisfy

$$\frac{\delta\sigma_{cl}}{\sigma_{cl}} \leq \frac{1}{4}\left[1 + \left(\frac{1+f_b R}{R\delta f_b}\right)\right]^{-1} \tag{5}$$

where

$$R = [N_{arc}(f_b = 1) - N_{arc}(f_b = 0)]/N_{arc}(f_b = 0).$$

For instance, if $R \sim 2$ and $f_b = 0.4$ and we require $\delta f_b \leq 0.2$, then $\delta\sigma_{cl}/\sigma_{cl} \leq 0.045$. This accuracy would require the measurement of ~ 1000 redshifts (Danese, de Zotti & Tullio 1980), a formidable task even in a local cluster, let alone one

at $z \sim 0.4$. X-ray temperature measurements to high precision might allow a determination of f_b to this accuracy. The different shapes of the predicted $\Phi(d_c)$ for the two hypotheses nevertheless suggest that, for a single cluster with *many* arcs, an analysis based on the *shape* of this distribution might enable us to test which of these hypotheses about $N(z)$ is the most likely. This approach will be discussed in the next section.

### 3.5 A likelihood ratio test based on $\Phi(d_c)$

Suppose a cluster has arcs with distortions larger than some chosen critical value A_c at distances $(d_1, d_2, \ldots, d_n)$ from the cluster centre. For an assumed σ_{cl} the singular isothermal sphere model can be used to predict the expected d_c distribution $\Phi(d_c | H_i, \sigma_{cl})$ under the hypothesis of a no-evolution $N(z)(H_0)$ or one with a fraction, f_b, of galaxies at high redshift (H_1). This $\Phi(d_c)$ yields the probability of observing the data $(d_1, d_2, \ldots, d_n)$, $p(d_1, \ldots, d_n | H_i, \sigma_{cl}) = p_i$ for short. Using the standard maximum likelihood method (Silvey 1975), one can estimate the cluster velocity dispersion. The σ which yields the greatest likelihood of observing the set of arcs is the *maximum likelihood estimator* $\hat{\sigma}$ of the cluster velocity dispersion. This estimator will depend on the assumed $N(z)$.

As an example consider the five arcs in A370 with $A > 1.5$. For a no-evolution $N(z)$ the radial positions of these arcs yield $\hat{\sigma} = 1200$ km s^{-1}, gratifying close to the optically determined value of 1367^{+310}_{-184} km s^{-1} for the red galaxies in A370 [the blue galaxies yield a larger velocity dispersion but there is some evidence that these are subclustered in velocity space, see Henry & Lavery (1987)]. The radial arc distribution is therefore an independent method for estimating cluster velocity dispersions, although the calculations rely on the assumed cluster potential and $N(z)$. Additionally we might have been fortunate in our estimate of the velocity dispersion of A370 since, for a small number of arcs (~ 6), the errors on the estimate of the velocity dispersion by this method can be as large as the errors in the dynamical estimate. However, as we will show, with a larger sample of arcs this estimator can be very accurate, and could provide a useful means of determining velocity dispersions of clusters at high redshift.

In this section the null hypothesis will be that the sources are distributed according to the no-evolution model to $V = 25$, and the alternate hypothesis will place a fraction f_b of the sources at $z = 2$ with the remainder distributed according to the no-evolution $N(z)$. Application of the maximum likelihood method to each hypothesis will yield two estimates of σ, denoted $\hat{\sigma}_0$ and $\hat{\sigma}_1$, and two probabilities $\hat{p}_0$, $\hat{p}_1$. If one of the inferred velocity dispersions is clearly unreasonable then the other hypothesis would be favoured. Since such a clear distinction is unlikely (for A370 H_0 yields 1200 km s^{-1} and for H_1 1075 km s^{-1}), the most sensible method for comparing the hypotheses is to construct the ratio $\Lambda = \hat{p}_0/\hat{p}_1$, the standard statistical likelihood ratio test of one hypothesis against another. If this ratio is large, one can safely reject the alternate hypothesis (a large fraction of sources at high redshift) in favour of the null (no evolution) hypothesis.

The important question now is how many arcs would be needed to distinguish confidently between these two hypotheses. In order to answer this question, several simulations have been made. These are described stepwise below.

(a) $N_{arc} = 6$ $A > 1.5$

(b) $N_{arc} = 40$ $A > 1.25$
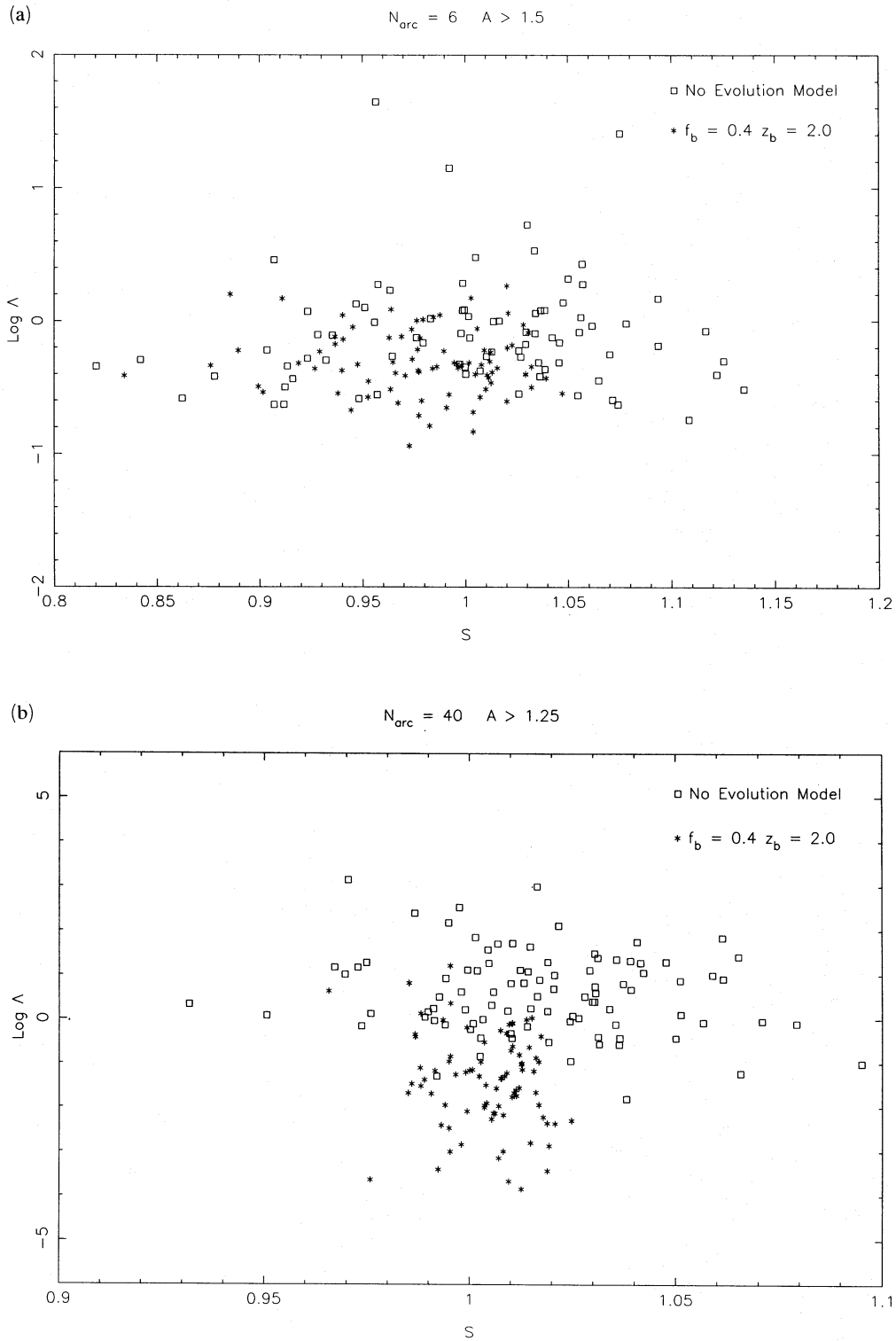
Figure 4. (a) The distribution of likelihood ratios and estimates of the cluster velocity dispersion for $N_{arc} = 6$. Square symbols correspond to arcs generated from a no-evolution $N(z)$ while the stars correspond to arcs generated with $f_b = 0.4$ and $z_b = 2.0$. (b) The distribution of likelihood ratios and estimates of the cluster velocity dispersion for $N_{arc} = 40$. Notice there is a much clearer separation of the components.

(1) Choose the cluster velocity dispersion σ_{cl} at random, and place the cluster at $z_{cl} = 0.4$.

(2) Generate N_{arc} arcs (with distortions above a specified critical A_c) using a singular isothermal sphere model with this velocity dispersion and the null $N(z)$ distribution (no evolution).

(3) Now calculate the likelihood of observing this set of arcs for a range of cluster velocity dispersions with the null hypothesis $N(z)$ *and* for a range of cluster velocity dispersions with the alternate redshift distribution described above.

(4) For each hypothesis determine the maximum likelihood estimates of σ_{cl} ($\hat\sigma_0$ and $\hat\sigma_1$). Calculate $\log_{10}\Lambda = \log_{10}(\hat p_0/\hat p_1)$ and $S = \hat\sigma_0/\sigma_{cl}$.

(5) Repeat the above procedure several times, resulting in a set of $(S, \log_{10}\Lambda)$ pairs.

(6) Now repeat the above simulations but in this case generate the set of N_{arc} arcs (stage 2) using the $N(z)$ of the alternate hypothesis. In this case the ratio S is defined as $S = \hat\sigma_1/\sigma_{cl}$ and $\log_{10}\Lambda = \log_{10}(\hat p_0/\hat p_1)$ as before.

Ideally then the values of $\log_{10}\Lambda$ in the first set of simulations should be greater than those in the second set, and the values of S in either case should be close to unity. Fig. 4(a) shows a plot of the 100 $(S, \log_{10}\Lambda)$ pairs for each type of simulation with $N_{arc} = 6$. The values of $\log_{10}\Lambda$ are similar for each hypothesis. Therefore a measurement of $\log_{10}\Lambda$ from a data set consisting of six arcs would not yield a test of H_0 against H_1. Fig. 4(b) shows the results for $N_{arc} = 40$, which clearly differentiate between the two hypotheses. Moreover, this approach also provides a very good estimate of the cluster velocity dispersion (typically to better than 5 per cent). In terms of defining precise significance levels for this test a larger simulation would be needed, but by inspection one can see that a value of $\log_{10}\Lambda > 1.0$ arises for only 1 per cent of the simulations with the redshift distribution of H_1, and thus, if the data have a measured value of $\log_{10}\Lambda > 1.0$, there is only at most a 1 per cent chance that we would be in error in choosing the null over the alternate hypothesis. Thus, with a set of 40 arcs in a single cluster, it should be possible to discriminate with some confidence between a no-evolution $N(z)$ and an $N(z)$ with 40 per cent of objects at $z = 2$. If f_b or z_b are larger, then this test becomes even more powerful.

4   DISCUSSION

There are several assumptions which must be discussed. The first is our use of the singular isothermal sphere model as the lens model. It is well known that determination of the mass distribution in clusters in a way free from assumptions is very difficult (see Fitchett 1990 for a review). Even the best-studied rich cluster, Coma, has a poorly constrained mass distribution. On the other hand, Beers & Tonry (1986) have shown that clusters have galaxy surface-density distributions which fall as r^{-1}. This finding is consistent with a singular isothermal sphere mass distribution if mass traces light in the centres of clusters.

If clusters really do have cores of constant density then their effect on our analysis will depend on their extent. Suppose the core has a size r_c, and that exterior to this region the cluster approximates the isothermal sphere density distribution $\rho \propto r^{-2}$. We need to compare the angular scale of the cluster core $\theta_{core} = r_c/r(z_{cl})$ with the lensing scale θ_{lens}. The

lens scale depends on the cluster velocity dispersion, its redshift, the redshift of the source population and on the size of A. For an intrinsically circular source to be distorted $> A$, its impact parameter must lie at

$$\theta_s < \theta_{lens} = \Delta (A-1)^{-1} \approx 42\,(\sigma/1200\ \mathrm{km\ s^{-1}})^2 (A-1)^{-1}$$
$$\times [1 - r(z_l)/r(z_s)]\ \mathrm{arcsec}.$$

This is the scale that must be compared to θ_{core}. For a cluster at $z_{cl} = 0.4$ and a typical source redshift of, say, $z = 2.0$, this gives $\theta_{lens} \sim 27\,(\sigma/1200\ \mathrm{km\ s^{-1}})^2 (A-1)^{-1}$ arcsec, which, for $A = 1.25$, gives $\theta_{lens} \sim 108\,(\sigma/1200\ \mathrm{km\ s^{-1}})^2$ arcsec. Now, for a cluster at $z = 0.4$, the angular scale of the core is $\theta_{core} \sim 55$ $(r_c/250\ \mathrm{kpc})$ arcsec. This is approximately half the lensing scale, and thus one would expect approximately 25 per cent of the images to have been lensed by the core. This fraction, while non-negligible, would not significantly alter the application of our method. This is because the core region will distort background objects less than in the singular case, and so some lensed images close to the cluster centre will not satisfy the distortion criteria and so not be in the sample on which the d_c distribution is based. Since the skewness of the $\Phi(d_c)$ distribution is towards large d_c, however, this should be preserved. We intend to check this analysis using nonsingular isothermal sphere models in our next paper. Of course, if the actual mass distribution were known in one cluster, the likelihood ratio test could be straightforwardly applied with confidence. The mass distribution in clusters will most likely be determined by measurements of the temperature and density profile of the hot X-ray emitting gas sitting in equilibrium in the cluster potential.

We now discuss the optimal strategy for carrying out our test. In principle the test can be applied with similar ease to
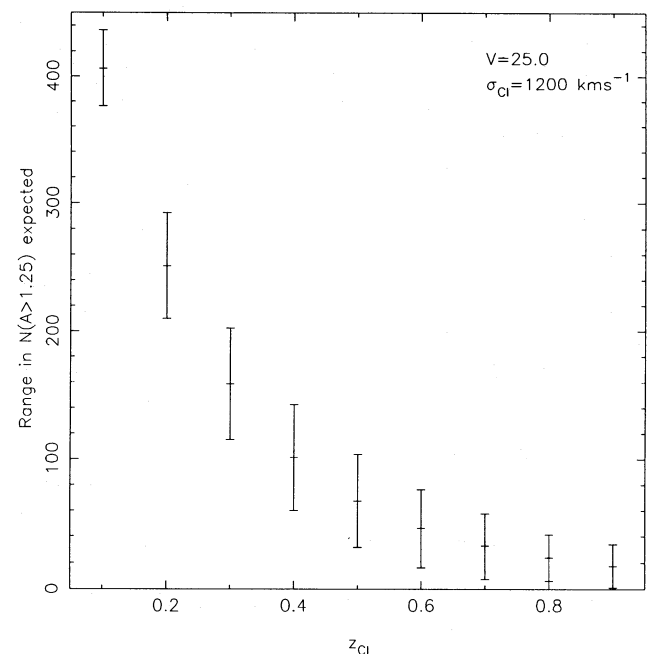
Figure 5. The range in the expected number of arcs with $A > 1.25$ seen in a cluster at various redshifts. The cluster has $\sigma_{cl} = 1200$ km s^{-1} and the range in the number of arcs corresponds to f_b increasing from 0 to 0.4 at $z_b = 2.0$ with the remaining fraction of galaxies, $(1 - f_b)$, distributed according to the usual no-evolution $N(z)$ to $V = 25$.

clusters at a range of redshifts since arc detection requires securing a certain signal-to-noise ratio for the *background* population. Nevertheless, there are several competing effects which suggest that the test is close to optimal for a cluster at $z_{cl} = 0.4$. For a low-redshift cluster (say $z_{cl} = 0.1$), the shapes of the $\Phi(d_c)$ curves are not as different for different values of f_b and z_b as they are for higher redshift clusters. This suggests using the highest redshift clusters known for such a test. At higher redshift, on the other hand, the number of arcs produced decreases whatever the postulated $N(z)$. This is shown in Fig. 5 where the range in the number of arcs produced with $A > 1.25$ as the fraction, f_b, of sources at $z_b = 2$ varies from 0 to 0.4 is plotted against the cluster redshift. Here the model cluster has a velocity dispersion of 1200 km s^{-1} and the source surface density is taken to be 27.6 arcmin^{-2}. This limit is readily achievable on a 4-m telescope. The declining number of arcs produced in clusters of higher redshift suggests that, unless a very rich cluster is available (recall $N_{arc} \propto \sigma_{cl}^4$), the optimal cluster for this test has $z \sim 0.4$.

5 CONCLUSIONS

We have searched for arc-like features in a homogeneous set of deep V images of 19 rich clusters of moderate redshift. 20 candidate arcs with $A > 2$ and six with $A > 3.5$ have been found. We have modelled the gravitational lensing effect of our ensemble of clusters on a background population of sources and find that the number of arcs and their shapes and orientations are consistent with the lensing hypothesis.

One aim of this paper was to explore whether data of this type (i.e. a few arcs in each of many rich clusters) could be used to set constraints on the redshift distribution of the faint background sources. We have shown that the number of arcs discovered above some critical distortion, or their radial distribution about the cluster centres, *could* constrain the redshift distribution of the sources if the cluster properties were well known, but very precise estimates of cluster velocity dispersions would be required to carry out these tests.

We have therefore explored the use of the radial distribution about the cluster centre of a larger sample of arcs as a possible probe of the faint galaxy redshift distribution. A high-redshift component of the faint galaxy population leads to a large fraction of arcs at large distances from the cluster centre, and a consequent skewness in the distribution of arc distances. We have devised a likelihood ratio test based on the *shape* of the radial distribution of arcs around the cluster centre. This test can discriminate between different redshift distributions for the background objects if ≥ 40 arclets can be found in one cluster.

Additionally this method should yield a very accurate measure (typically to better than 5 per cent) of the cluster velocity dispersion, which can be found for a cluster at *any* redshift (provided only that there are enough arclets). This approach to determining cluster velocity dispersions could prove extremely interesting as a means of constraining theories of galaxy formation, since it has recently been claimed that the abundance of high-redshift clusters with high purported velocity dispersions provide a strong argument against the cold dark matter theory of galaxy formation (Evrard 1989; Peebles, Daly & Juszkiewicz 1990). These analyses, based on spectroscopically determined velocity dispersions, are subject to the usual projection-effect problems.

The lensing method avoids that problem and yields more accurate velocity dispersions per unit allocation of telescope time.

Clearly there are other factors that this analysis has not taken into account, for example the possibility of more complex cluster mass distributions and intrinsic ellipticity in the source population (Kochanek 1990). These issues will be addressed in future papers. It is clear that gravitational lensing offers a new and independent probe of the background galaxy population. With a better understanding of the lensing clusters, important cosmological applications will be possible.

REFERENCES

Abell, G. O., 1958. *Astrophys. J. Suppl.*, **3**, 211.
Abell, G. O., Corwin, H. G. & Olowin, R. P., 1989. *Astrophys. J. Suppl.*, **70**, 1.
Beers, T. C. & Tonry, J. L., 1986. *Astrophys. J.*, **300**, 557.
Broadhurst, T. J., Ellis, R. S. & Shanks, T., 1988. *Mon. Not. R. astr. Soc.*, **235**, 827.
Colless, M., Ellis, R. S., Taylor, K. & Hook, R. N., 1990. *Mon. Not. R. astr. Soc.*, **244**, 408.
Couch, W. J. & Sharples, R., 1988. *Mon. Not. R. astr. Soc.*, **229**, 423.
Couch, W. J., Hansen, L. Jørgensen, H., Nørgaard-Nielsen, H. U., Ellis, R. S. & Aragón-Salamanca, A., 1989. In: *Particle Astrophysics: Forefront Experimental Issues*, p. 192, ed. Norman, E. B., World Scientific, Singapore.
Couch, W. J., Ellis, R. S., Malin, D. F. & Maclaren, I., 1990. Preprint.
Cowie, L. L. & Lilly, S. J., 1990. In: *The Evolution of the Universe of Galaxies*, p. 212, ed. Kron, R., Astr. Soc. Pacif. Conference Series.
Cowie, L. L., Lilly, S. J., Gardner, J. & MacLean, I., 1989. *Astrophys. J.*, **332**, L29.
Danese, L., de Zotti, G. & Tullio, G., 1980. *Astr. Astrophys.*, **82**, 322.
Efstathiou, G., Ellis, R. S. & Peterson, B. A., 1988. *Mon. Not. R. astr. Soc.*, **232**, 431.
Ellis, R. S., 1990. In: *Gravitational Lenses*, p. 236, eds Mellier, Y., Fort, B. & Soucail, G., Springer Verlag, Berlin.
Evrard, A. E., 1989. *Astrophys. J.*, **341**, L71.
Fitchett, M. J., 1990. In: *Clusters of Galaxies*, p. 111, eds Oegerle, W. R., Fitchett, M. J. & Danly, L., Cambridge University Press, Cambridge.
Fort, B., 1990. In: *Gravitational Lenses*, p. 221, eds Mellier, Y., Fort, B. & Soucail, G., Springer Verlag, Berlin.
Fort, B., Prieur, J.-L., Mathez, G., Mellier, Y. & Soucail, G., 1988. *Astr. Astrophys.*, **200**, L17.
Grossman, S. A. & Narayan, R., 1988. *Astrophys. J.*, **324**, L37.
Guhathakurta, P., Tyson, J. A. & Majewski, S. R., 1991. *Astrophys. J.*, **357**, L9.
Hansen, L., Nørgaard-Nielsen, H. U. & Jørgensen, H. E., 1987. *ESO Messenger*, **47**, 46.
Hansen, L., Nørgaard-Nielsen, H. U., Jørgensen, H. E., Ellis, R. S. & Couch, W. J., 1989. *Astr. Astrophys.*, **211**, L9.
Henry, J. P. & Lavery, R., 1987. *Astrophys. J.*, **323**, 473.
Kochanek, C. S., 1990. Preprint.
Koo, D. C., 1989. In: *Epoch of Galaxy Formation*, p. 71, eds Frenk, C. S. *et al.*, Kluwer Academic Press, Dordrecht.

Lavery, R. & Henry, J. P., 1988. *Astrophys. J.*, **329**, L21.

Lynds, R. & Petrosian, V., 1989. *Astrophys. J.*, **336**, 1.

Nemiroff, R. J. & Dekel, A., 1989. *Astrophys. J.*, **344**, 51.

Nørgaard-Nielsen, H. U., Hansen, L., Jørgensen, H. E., Aragón-Salamanca, A., Ellis, R. S. & Couch, W. J., 1989. *Nature*, **339**, 523.

Peebles, P. J. E., Daly, R. A. & Juszkiewicz, R., 1990. *Astrophys. J.*, **347**, 563.

Phillipps, S., Disney, M. J. & Davies, J., 1990. *Mon. Not. R. astr. Soc.*, **242**, 235.

Silvey, S. D., 1975. *Statistical Inference*, Chapman & Hall, London.

Soucail, G., Mellier, Y., Fort, B., Mathez, G. & Cailloux, M., 1988. *Astr. Astrophys.*, **191**, L19.

Soucail, G., Mellier, Y., Fort, B., Matthez, G. & Cailloux, M., 1990. In: *Gravitational Lenses*, p. 291, eds Mellier, Y., Fort, B. & Soucail, G., Springer Verlag.

Turner, E. L., Ostriker, J. P. & Gott, J. R., 1984. *Astrophys. J.*, **284**, 1.

Tyson, J. A., 1988. *Astr. J.*, **96**, 1.

Tyson, J. A., Valdes, F. & Wenk, R. A., 1990. *Astrophys. J.*, **239**, L1.